Applied Acoustics 130 (2018) 222–229

Contents lists available at ScienceDirect

Applied Acoustics

journal homepage: www.elsevier.com/locate/apacoust

Leveraging the arrangement of multiple, critically constrained inclusions in resonant metamaterials for control of broadband vibroacoustic energy

Justin Bishop, Ryan L. Harne*

Department of Mechanical and Aerospace Engineering, The Ohio State University, Columbus, OH 43210, USA

A B S T R A C T

In many applications, unwanted vibroacoustic energies are broadband and concentrated at low frequencies, which presents a challenge for resonance-based dampers and lightweight materials to abate such energies. Recent studies have shown that utilizing the elastic stability limit in elastomeric inclusions can lead to a theoretically unbounded increase in macroscopic damping properties. Additionally, by embedding multiple, distributed masses within poroelastic media, the ability of the media to suppress acoustic energy is increased beyond the inherent attenuation characteristics of the foam itself. To understand the interaction between these two phenomena, this research experimentally characterizes the influences of strategically arranging multiple, critically constrained inclusions to tailor the vibroacoustic damping properties of poroelastic, resonant metamaterials. It is found that that such metamaterials are more effective when two adjacent inclusions are more widely spaced in the axis of wave propagation and in different planes orthogonal to the plane wave. The evidence also suggests that inclusions aligned in the axes normal to the wavefront direction especially promote vibroacoustic energy absorption. Arrangements of multiple inclusions are demonstrated to be robust, in that non-ideal, inclusion designs lead to metamaterials that remain effective to attenuate broadband energy. Moreover, these engineered inclusions are compared to traditional solid inclusions, and are shown to have similar or greater energy suppression while using around 40% less mass.

1. Introduction

In vehicle systems applications, vibroacoustic energy often originates from spectrally broadband sources of noise such as aeroacoustic perturbations, tire-road interactions, and powertrain [1]. Low frequency vibrations are particularly difficult to dissipate with minimal mass due to the longer wavelengths of such frequencies [2] and ineffectiveness of traditional, lightweight acoustic foams (poroelastic media) in this frequency band [3]. As a result, vibroacoustic energy absorption or attenuation methods and materials have received significant attention over the years [4]. Frequency selective attenuation properties are achieved in resonant metamaterials via absorption phenomena in tunable bandgaps [5,6]. Yet, these properties are often parameter sensitive and narrowband, which makes them ineffective in scenarios that require robust, broadband energy attenuation. Many proposed resonant metamaterials are also made of dense materials including metals [7] and heavy rubbers [8,9], which are impractical when the added mass of the treatment counterbalances the performance requirements of the application, such as light-weighting demands for vehicle systems.

Researchers have additionally begun to utilize buckling instability to achieve exceptional and tunable energy attenuation properties. Shan et al. [10] and Pal et al. [11] have demonstrated that energy attenuation and wave propagation directionality are greatly tailored in metamaterials having internal lattice architectures that deform and buckle according to the pre-load. Yet, because such phenomena rely on threshold energy inputs to enable the absorption or capture properties [12–14], the sensitive relation between the desired metamaterial behavior and excitation source discourages the use of the concept when robust properties are required in the face of uncertain input energies. In fact, while buckling phenomena may enhance the energy attenuation of vibroacoustic metamaterials, utilizing the critical bifurcation point of buckling itself should theoretically provide greater energy suppression behaviors [15] due to the cancellation of the positive and negative stiffnesses [16]. Recent investigations on critically constrained metamaterials have demonstrated first realizations of such desirable properties in robust elastomeric architectures. This contrasts with reliance on careful temperature or electric field tuning [17,18] in prior studies on two-phase composites and ferroelectrics configured to promote novel dissipation properties near critical points. These critically

* Corresponding author.
E-mail address: harne.3@osu.edu (R.L. Harne).

http://dx.doi.org/10.1016/j.apacoust.2017.10.003
Received 31 May 2017; Received in revised form 12 August 2017; Accepted 2 October 2017

constrained metamaterials are recently shown to provide extreme resilience to impact energy [19] to greater extent than post-buckled metamaterials and with less mass than traditional bulk material dampers.

Inspired by observations of enhancement of poroelastic media acoustic wave attenuation properties via lumped mass inclusions [20–24], the concept of critically constrained elastomeric inclusions was applied with the aim to enhance low and broadband frequency attenuation properties of the host poroelastic metamaterials [25]. In this work, the authors found that critical point constraints best cultivate vibroacoustic energy suppression characteristics in the acoustic foams in absorption coefficient and elastic wave transmission experiments [25], in agreement with the theoretical premise. On the other hand, only a single inclusion was applied in a given metamaterial specimen [25], so that opportunities to leverage multiple, strategically arranged inclusions were untested. This is despite the fact that studies on phononic crystals [9] and on lumped mass inclusions in poroelastic media [24] have revealed notable benefits to the attenuation properties by harnessing arrangements of resonant inclusions. Moreover, the influences of interactions between and among multiple constrained inclusions remains unknown [25], while comparable evaluations of lumped mass resonant inclusions suggest interaction phenomena are pivotal towards determining the metamaterial effectiveness at broadband energy attenuation [21]. A similar class of metaporous materials has been modeled and reported to cultivate broadband wave absorption due to a combination of elastic deformation in thin-shelled elastic inclusions and visco-thermal dissipation in the poroelastic host medium [26]. These metaporous materials have a rigid backing [27] that prevent wave transmission. In contrast, the metamaterials with critically constrained inclusions transmit and reflect acoustic wave energy in extents tunable according to the inclusion type [25]. Yet, how to leverage the inclusion characteristics and placements to capitalize upon the wave attenuation capabilities have yet to be determined.

To assess how multiple inclusion arrangement and the resulting interaction phenomena tailor the advantages of critically constrained inclusions in resonant metamaterials, this research undertakes a detailed experimental study to characterize how such parameters tailor the acoustic wave absorption and transmission properties of the host poroelastic media. The following section reviews the design and fabrication strategies of the inclusions and resulting metamaterials. Then, the results of extensive experiments are reported and insights on the roles of inclusion placements and interaction that are uncovered from the measurements are discussed. Finally, concluding remarks summarize the key findings of this research.

2. Design and fabrication of inclusions and metamaterials

The critically constrained inclusions utilized in this report are designed and fabricated in ways comparable to the elastomeric inclusions recently investigated by the authors [25]. Readers with greater interest in the complete fabrication procedures are referred to the prior work [25]. The design of the elastomeric, engineered inclusions with rotationally symmetric void structures involves several geometric parameters although only two parameter ratios are independent after the number of voids is selected. The inset of Fig. 1 illustrates the cross-section geometry of the engineered inclusions. The rotationally symmetric internal void architecture, with outer diameter d_o, gives rise to global, rotational buckling when constrained in the metallic shell of diameter d_i that is smaller than d_o. This contrasts with local buckling phenomena that occur either for non-rotationally symmetric voids [14] or when the constraining loads are not circumferential [28]. The ratio of outer to inner diameters is one design feature that governs the nearness to the critical point of buckling. The second significant design feature of interest in this report is the ratio of open to solid angle. This angle ratio is schematically shown in the inset of Fig. 1 by the ratio of the void angle α to the solid angle β. The solid angle is prescribed

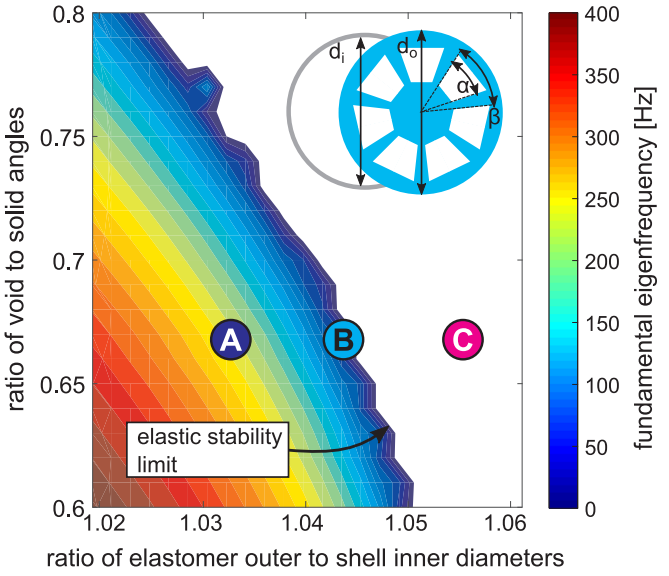

Fig. 1. FE model results of real part of fundamental eigenfrequency for given cross-section geometry of constrained, elastomeric, engineered inclusion. The horizon between shaded and unshaded regions of the contour denote the elastic stability limit (the critical point of buckling). Inset shows the engineered inclusion cross-section geometry.

according to the number N of voids, via $\beta = 2\pi/N$. In this study, $N = 7$. Variation of the open angle ratio tailors the thickness of the radially arrayed beams.

In this research, a parametric, plane strain finite element (FE) study is conducted in COMSOL Multiphysics to select the design parameter ratios for the engineered inclusions to be fabricated and experimentally examined. In the FE simulations, both open angle ratio and diameter ratio are adjusted over the range of values that can be fabricated. The diameter ratio is realized by a circumferential compression applied to the elastomeric material cross-section. The linear elastic material properties include the Young's modulus 752 kPa, the Poisson's ratio 0.49, and the density 1145 kg/m^3. Eigenfrequency studies are undertaken in the FE model to characterize the extent to which the engineered inclusion geometry (by open angle ratio) and constraint (by diameter ratio) result in nearness of the elastomeric architecture to the point of buckling. By plotting the real part of the fundamental eigenfrequency in Fig. 1, the design parameter ratios that induce critical point constraints on the inclusions are seen as the horizon between the shaded and unshaded areas of the contour. The unshaded areas correspond to an imaginary eigenfrequency for this linear elastic FE model, which subsequently corresponds to a post-buckled inclusion geometry [29].

For the open angle ratio of 0.67, Fig. 1 indicates three, engineered inclusion geometries that are selected for fabrication using the labels of A, B, and C. The inclusion geometries are made such that they result in diameter ratios of 1.0325, 1.0455, and 1.0547, respectively, when compressed within the aluminum metal shells. The inclusion A is compressed by its diameter ratio to an extent that is insufficient to induce buckling, the inclusion B is near to the critical point of buckling, and while C is plainly post-buckled. These aspects may be observed in Fig. 2(a). The photographs compare the engineered inclusions against a control inclusion realized from as a solid cylinder of the same elastomer used to fabricate the engineered inclusions. Whether engineered or control, each inclusion is placed into an aluminum shell of inner diameter $d_i = 16.56$ mm and thickness great enough such that circumferential constraints induced for the engineered inclusions are near ideal. Recall that a global rotation deformation is associated with the post-buckling of these rotationally symmetric cross-section geometries [25,28]. In the photographs of Fig. 2(a), the engineered inclusions A, B, and C are shown to exemplify that they respectively undergo no

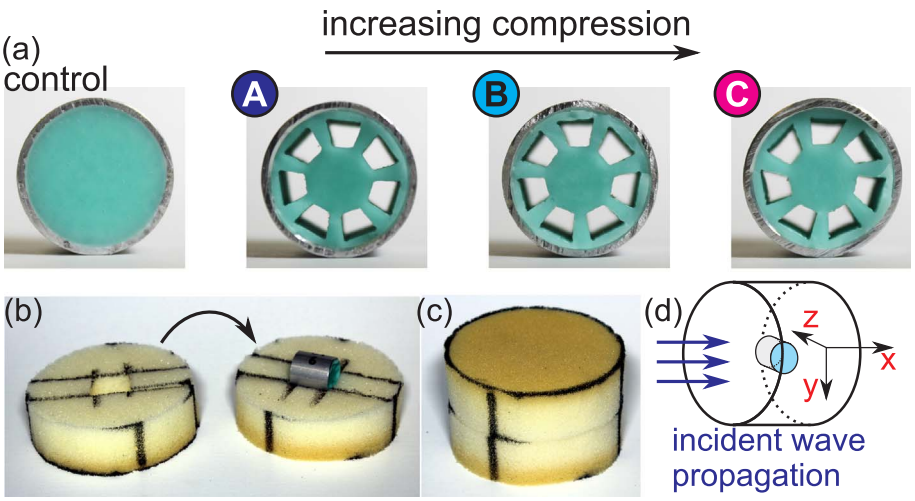

Fig. 2. (a) Control inclusion and engineered inclusions A, B, and C. (b) Assembly and bonding method of inclusions in poroelastic foam. (c) A resonant metamaterial specimen. (d) Notation of inclusion placement respecting the x-axis of wave propagation.

Table 1
Comparison of inclusion mass, with and without the constraining shells.

Specimen	Control	A	B	C
Elastomer mass [g]	4.846 (–)	2.916	2.759	2.815
(% < control)		(39.8%)	(43.1%)	(41.9%)
Shell and elastomer mass	8.437 (–)	6.500	6.342	6.400
[g] (% < control)		(23.0%)	(24.8%)	(24.1%)

rotation (A), very slight rotation (B), and evident rotation (C). These observations are in agreement with the design guidance of the FE model respecting Fig. 1 predictions. Because the engineered elastomeric inclusions use the same open angle ratio of 0.67, only the diameter ratio influences the nearness to buckling for the specimens considered in this report. For comparison, Table 1 presents the masses of the inclusions studied in this report. Each value in the table is a mean across the multiple samples of each inclusion type created, since certain experimental studies presented here utilize multiple inclusions in given poroelastic metamaterials. It is evident that around a 40% mass reduction is realized via the engineered inclusions respecting the control, while the introduction of the constraining shell tailors the mass reduction to around 24% for the engineered inclusions. Arrangements of two engineered inclusions considered in this study are 131.7% more massive than the foam sample on average, while the control samples with two inclusions are 169.8% more massive than the foam sample on average. Considering the rigorous demands for light-weighting in vehicle systems applications while maintaining large suppression of the low and broadband frequency vibroacoustic energies [1], the opportunity to use the engineered inclusions in resonant metamaterials to suppress the same or greater excitation energies as that achieved with the heavier control inclusions may be of promising, practical potential.

The control and engineered inclusions are then used to realize resonant metamaterials via their insertion (or embedding) into a host elastic media. Here, poroelastic, polyurethane foam samples (Foam Factory Super Soft Foam) are cut to cylindrical dimensions of 100 mm length and 85 mm diameter, and then cut in half along the lengths where inclusions will be inserted. From each half, a triangular wedge of foam is removed. The portions of the remaining channel wherein an inclusion will be placed are left empty, while the wedge is cut down to size and reinserted around these locations. This process is photographically shown in Fig. 2(b), which illustrates a fabrication method for a specimen that includes one engineered inclusion. A light amount of spray adhesive is used on all cut surfaces to ensure the foam and inclusion are amply held together once reassembled as a total metamaterial specimen, as seen in Fig. 2(c). In this report, inclusions are always embedded into the poroelastic media so that the constant cross-section axis of the inclusion is aligned with the z-axis, as shown in Fig. 2(d). This is because the inclusion internal geometry enhances compliance of the elastomeric mass core more so when the constrained inclusion is acted upon by stresses in the x- or y-axes [19,28]. For specimens with multiple inclusions, multiple channels are cut or multiple inclusions are placed into each channel, depending on the configuration of the specimen, using procedures similar to those described above and shown in Fig. 2(b). This host foam has a density of 19.2 kg/m^3, as listed by the manufacturer. Poisson's ratio and porosity are assumed to be 0.44 and 0.99, respectively, which are within the range of similar foams [30]. Young's modulus of the foam is measured via load frame examinations to be 20.3 kPa.

3. Experimental assessment of vibroacoustic energy attenuation properties

To assess the influences of the different inclusion types, the use of multiple inclusions, and the organized arrangement of the inclusions within the poroelastic media, experiments are conducted to quantify force (elastic wave) transmission, acoustic energy absorption, and acoustic energy transmission through the metamaterial specimens. The following sub-sections describe the experiments and detail the findings that illuminate strategies for best leveraging these characteristics of resonant metamaterials with engineered inclusions for broadband vibroacoustic energy control.

3.1. Influence of spacing between two inclusions in the axis of wave propagation

Force transmissibility through the specimens is evaluated in the laboratory via the following experimental setup. An electrodynamic shaker and amplifier (Labworks LT-140-110, PA-141) are used to excite the metamaterial specimens with low level Gaussian white noise. An accelerometer (PCB 352C33) signal is used by a shaker controller (Vibration Research VR 9500) to govern the white noise root mean square (RMS) acceleration level 0.1 m/s^2 produced at the shaker. A force transducer between the shaker and specimen (PCB 208C02) measures the input force, while a second force transducer (PCB 208C01) between the specimen and a rigid termination measures the output force. Force expander plates on the incoming and outgoing sides of the specimens ensure that the force delivery and transmission are concentrated ideally on the transducers [25]. The Gaussian white noise delivered to the metamaterial specimens is controlled across the frequency band of 20–600 Hz, and held at the target RMS level until 60 s of data are collected and then averaged over 1-s spans, with 50% overlap windowing used in the computation of the force

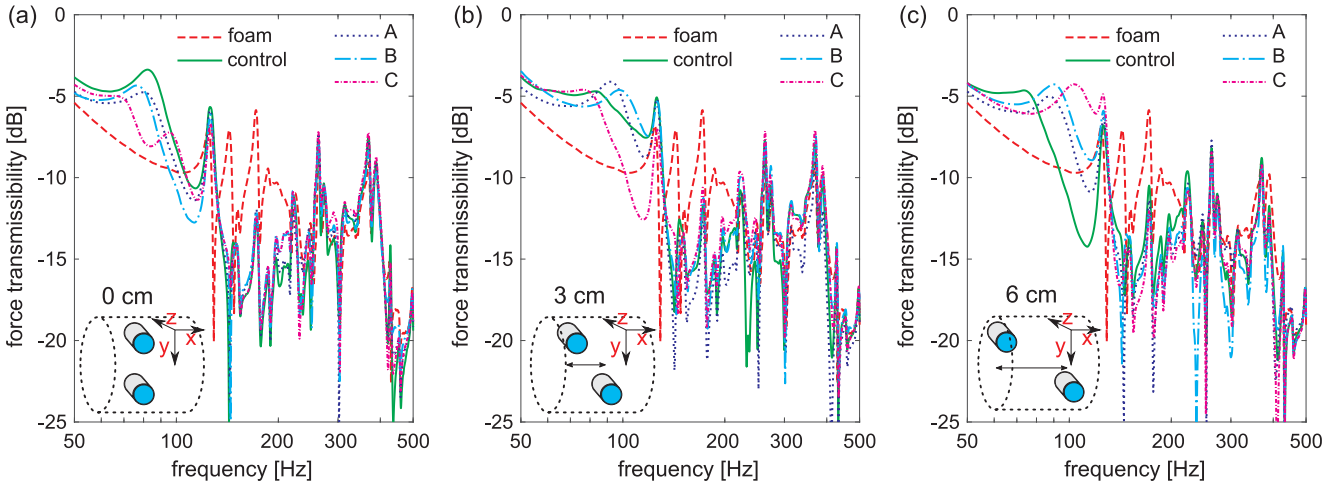

Fig. 3. Force transmissibility for two inclusions with (a) 0 cm spacing, (b) 3 cm spacing, and (c) 6 cm spacing along the axis of wave propagation.

transmissibility in the frequency domain. All resonant metamaterial specimens are examined in this way, whether containing the control or engineered inclusions, while samples of poroelastic foam of the same dimensions as the metamaterials are also evaluated to provide a baseline measure of force transmission.

Rigid inclusions in poroelastic media have been found to exhibit an effective footprint over which the dynamic behavior of the inclusion within the media may influence other inclusions embedded nearby [21]. To investigate the footprint of the engineered inclusions in this research, two inclusions are placed in the y-z plane, spaced by 38 mm in the y-axis, within a 100 mm long by 85 mm diameter sample of foam, see the inset of Fig. 3(a). Other specimens are fabricated that locate the inclusions with spacing distances of 3 or 6 cm in the x-axis, as shown in the insets of Fig. 3(b) and (c), respectively. Together, the evaluation of the force transmission through these metamaterials quantifies how inclusions interact within the metamaterials along the axis of wave propagation, yet in different x-z planes, with respect to the ability to tailor the transmitted force.

As shown in all plots of Fig. 3 for the resonant metamaterials, the mass from the inclusions in the metamaterial specimens causes a resonance in the region of 50–125 Hz when compared to the force transmitted through the foam itself (red[1] dash c

urve). It is also found that the resonance changes based on the inclusion architecture and the spacing between inclusions. The resonance peak tends to occur at a higher frequency when the inclusions are spaced apart by 3 cm than 6 cm in the x-axis, and is lowest in frequency when the inclusions remain in the same y-z plane. From approximately 150–500 Hz, force transmissibility tends to decrease with the addition of two inclusions. Above 500 Hz, the minute dynamics of the force expander plates are more prominent than the greatly diminished force transmission through the specimens so that the force transmission associated with the specimens above 500 Hz is effectively negligible. It is seen in Fig. 3(a) that the control inclusions and each of the engineered inclusions show a similar response in the 150–500 Hz band. This indicates that the interaction phenomena among embedded inclusions predominates the broadband force transmission from around 150–500 Hz, in contrast to the selection of or constraint on the inclusions. In contrast, the inclusion type has much greater influence on force transmissibility for the 3 cm spacing in Fig. 3(b) and the most influence on force transmissibility for the 6 cm spacing in Fig. 3(c). Specifically, whether spaced in the x-axis by 3 or 6 cm, the engineered inclusions transmit less force in the bandwidth of 150–280 Hz than the control inclusions. These results from the narrowband plots of Fig. 3 suggest that using multiple engineered inclusions to control the transmitted force through the metamaterials is best achieved by staggering inclusion placement in the wave propagation axis while locating them in different x-z planes.

Towards suppressing the force across a broad range of frequencies, the one-third octave band summations across the lower and upper frequency ranges shown in Fig. 3 are computed. Examining the cumulative force transmitted in the lower frequency band 44–140 Hz assesses resonant energy transmission, while the comparison from 140 to 560 Hz evaluates the effectiveness of the broadband attenuation at frequencies sufficiently greater than low order resonant states of the inclusions in the poroelastic media. The one-third octave band metrics are presented in Fig. 4 for (a) the lower frequency band of 44 to 140 Hz, and (b) the upper frequency band of 140–560 Hz. In Fig. 4(a), the magnitude of the cumulative transmitted force is around 5 to 6 dB regardless of the selection of the inclusions or their placement along the x-axis. This suggests that the resonant amplitudes of transmitted force are primarily governed by global dynamics of the inclusions as lumped masses [21] and are less dependent on interactions between inclusions. In the higher frequency band, Fig. 4(b), the cumulative transmitted force is less for the resonant metamaterials that place the inclusions apart by 6 cm in the x-axis, with the minor exception of the engineered specimen A. This reduction in cumulative one-third octave bands means that metamaterials with adjacent inclusions better suppress broadband, high frequency vibration energy when the inclusions are more greatly spaced apart in the x-axis while not remaining in the same x-z plane, confirming the conclusion drawn from the narrowband data. Moreover, by this approach, the resonance is not significantly changed, so that there are no apparent drawbacks to resonant energy transmission by strategically selecting the inclusion spacing for enhanced high frequency attenuation.

3.2. Influence of arrangement of two inclusions

In the experiments reported in Section 3.1 according to the inset of Fig. 3(a), the inclusions are arranged in a configuration here termed "1 × 2 × 1" because one inclusion is placed along the x-axis, two inclusions placed along the y-axis, and one inclusion placed along the z-axis of the metamaterial. Attention is then turned to investigate the interactions that may occur among inclusions arranged in different configurations within the poroelastic media. Based on size limitations of embedding the inclusions in the poroelastic foam without placing inclusions too near the periphery of the metamaterial that may lead to extraneous edge effects [21,24], in this section the spacing between two inclusions in the x-axis is 50 mm center-to-center for 2 × 1 × 1

[1] For interpretation of color in Fig. 3, the reader is referred to the web version of this article.

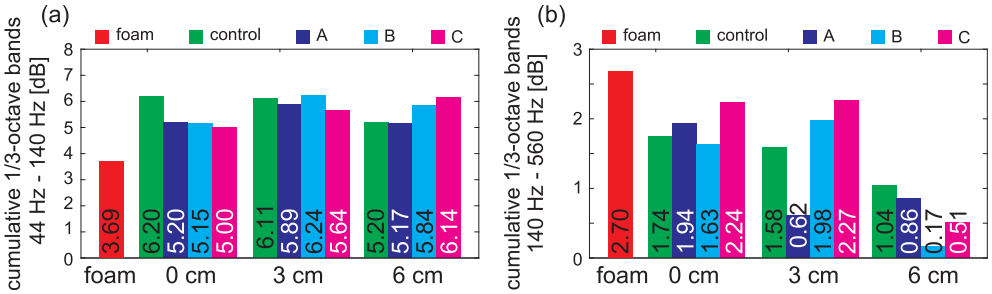

Fig. 4. Cumulative one-third octave bands for (a) lower band of 44–140 Hz and (b) upper band of 140–560 Hz.

arrangements, while the similar spacings in the y- and z-axes are 38 mm center-to-center, respectively for 1 × 2 × 1 and 1 × 1 × 2 arrangements.

3.3. Effects upon acoustic properties

To quantify the absorption coefficient and transmission loss of the specimens, cylindrical impedance and transmission loss tubes are utilized according to ASTM standards [31,32]. The tube used in the laboratory is convertible between measurement modes for impedance and transmission loss. This setup allows for samples with a finite number of inclusions to be studied, in contrast to a square cross section impedance tube whose rigid boundaries and geometry approximate periodic boundary conditions and hence infinitely repeating layers [24]. In the experiments of this work, the samples are slightly oversized relative to the tube inner diameter to create a sufficiently tight seal at the tube walls that prevents direct wave transmission around the specimens. The acoustic source upstream of the specimens is a 4 in. (102 mm) diameter loudspeaker driven by Gaussian white noise from an amplifier (AudioSource AMP100). Pressure signals obtained from microphones (PCB 130E20) utilized in the experiments are recorded for 40 s and then digitally bandpass filtered prior to computing the relevant transfer functions [31,32], using 50% overlap and windowing for each calculation across 1-s time intervals.

Absorption coefficient and transmission loss are presented in Fig. 5(a) and (b), respectively, for the 1 × 2 × 1 arrangement. It is seen in Fig. 5(a) that absorption coefficient increases above the inherent absorption of the foam itself with the addition of two inclusions of any type. The selection of the inclusions reveals a moderate influence on how much acoustic energy is absorbed by the metamaterial. For example, the metamaterial with 1 × 2 × 1 arrangement of the engineered inclusions A enhances absorption coefficient from 300 to 400 Hz by an absolute value of almost 0.03, and peaks at near perfect absorption of acoustic waves around 700 Hz. These enhancements come with a drawback of reduced acoustic wave absorption in the band around 900–1300 Hz than even the foam itself or the resonant metamaterial with control inclusions. Such tradeoffs are to be considered along the fact that the engineered inclusions use around 40% less mass than the control inclusions. Considering Fig. 5(b), the transmission loss is also affected by inclusion architecture, although the absolute changes observed are not significant, e.g. around 1 dB at any given frequency. In general, the results of Fig. 5 show that the resonant inclusions of the metamaterials can enhance wave absorption in and attenuation through the host poroelastic media. On the other hand, the results indicate that the poroelastic foam itself is a predominant factor in such properties at frequencies less than around 2 kHz since the absolute shifts in the metrics are not great. Indeed, this may be observed in data reported elsewhere in the literature considering broadband attenuation metrics when metamaterials utilize acoustic foams as the host media [23,24]. While the metamaterials utilizing the 2 × 1 × 1 and 1 × 1 × 2 arrangements of resonant inclusions are also measured, the absorption coefficient and transmission loss trends are not significantly different than those reported for the arrangement 1 × 2 × 1 and are thus not presented for brevity sake. This also corroborates the conclusion that the low frequency acoustical properties of the polyurethane foam considered in this investigation are more greatly influenced by the host poroelastic media and are less influenced by the presence of two resonant inclusions.

3.4. Effects upon force transmissibility

Since the adaptation of acoustic properties is not greatly altered by the differing arrangements of inclusions in the metamaterials, attention is then turned to the means for arrangement selection to tailor the

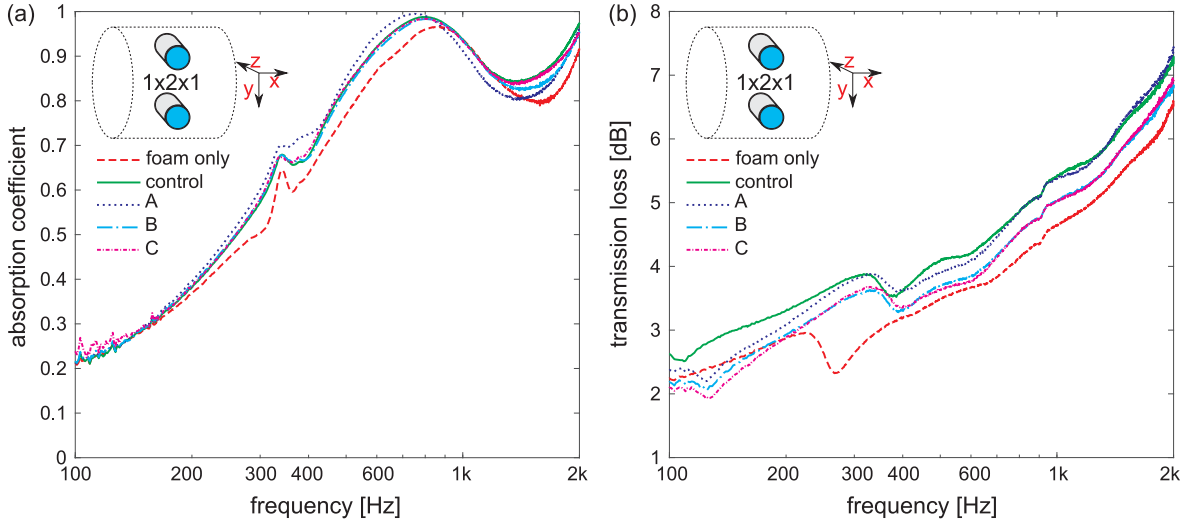

Fig. 5. 1 × 2 × 1 arrangement of inclusions (a) absorption coefficient and (b) transmission loss.

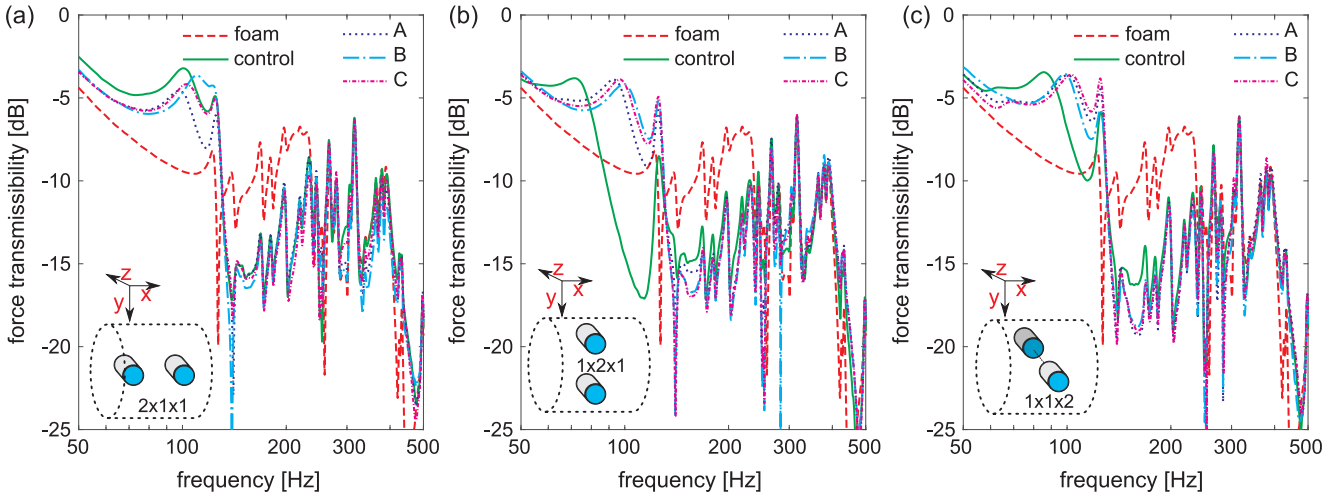

Fig. 6. Force transmissibility for (a) 2 × 1 × 1 arrangement, (b) 1 × 2 × 1 arrangement and (c) 1 × 1 × 2 arrangement.

broadband, low frequency force transmission through the systems. Using the experimental method described in Section 3.1, the metamaterials are examined to quantify the force transmissibility, and results are shown in Fig. 6. For the 2 × 1 × 1 arrangement in Fig. 6(a), the different inclusions yield similar force transmission characteristics in the narrowband comparison across frequencies 150–500 Hz. When compared to the control inclusions, the engineered inclusions lead to lower resonance amplitudes at frequencies below about 150 Hz, which may be in part due to their decreased mass that governs the lumped, lowest order dynamic behavior of the embedded elements [21]. For the 1 × 2 × 1 arrangement in Fig. 6(b), there is greater change in force transmissibility in the band of 140–280 Hz among the metamaterials having different inclusion types. The engineered inclusions clearly decrease force transmissibility by more than the control elastomer inclusions in this frequency band using the 1 × 2 × 1 arrangement of two inclusions. Yet, considering the force transmissibility measured for the 1 × 1 × 2 arrangement of inclusions, Fig. 6(c), there is less distinction of narrowband force transmission characteristics among the engineered, resonant metamaterials although the force transmissibility is evidently reduced from the levels achieved with the metamaterials having the control inclusions, particularly from around 140–200 Hz.

Fig. 7 presents the narrowband force transmissibility measurements consolidated so as to clearly compare metamaterials having the same type of inclusions but with such inclusions in different arrangements. It is seen that the 1 × 1 × 2 arrangement generally leads to the least force transmissibility in the frequency band 150–500 Hz, regardless of the type of inclusion in the resonant metamaterial. Considering these findings alongside the results of Figs. 3 and 4 for the 1 × 2 × 1 arrangement where spacing of the 2 inclusions in the x-axis (while in different x-z planes) led to greater reduction of force transmission, a concept of a “screen” of embedded inclusions may be suggested as a useful approach to enhance the force attenuation characteristics. In other words, arranging inclusions in 1 × 2 × 1 and 1 × 1 × 2 configurations or a 1 × 2 × 2 grid may be a valuable means to capitalize on the fewest number inclusions in the metamaterial to more substantially reduce transmitted force in a broadband way. The use of a square cross section impedance tube to mimic an infinite plane of inclusions may allow for reinforcement of this finding [33,34], and may enable continued study into ideal spacing between inclusions through adjustment of the unit cell size.

To examine how these findings of broadband frequency attenuation characteristics are specifically tailored according to the specific inclusion type, the one-third octave bands are computed and cumulative sums from “lower” and “upper” bands are taken, respectively, from 44 to 140 Hz and from 140 to 280 Hz. As shown in Fig. 8(a), the overall force transmitted around frequencies associated with the resonance tends to be between 6 dB and 7 dB regardless of the inclusion type or arrangement. On the other hand, the magnitude is slightly lower for most of the 1 × 2 × 1 arrangements than the other arrangements. Considering the upper frequency band, Fig. 8(b) clearly shows that broadband vibroacoustic energy is more greatly suppressed by the resonant metamaterials with 1 × 1 × 2 arrangements of engineered inclusions than for the control inclusions. Also, the 2 × 1 × 1 arrangement is the least effective at reducing force transmissibility from 140 to 280 Hz, Fig. 8(b). This finding agrees with the conclusion reached according to the results of the narrowband plots of Fig. 7. Indeed, the results of Fig. 8 further support the suggestion that 1 × 2 × 1 or 1 × 1 × 2 arrangements of inclusions are more effective at broadband vibroacoustic energy attenuation according to the arrangement approach of establishing a screen in the y-z plane through which the incident wave energy must pass in the x-axis. As a result, a greater amount of wave energy is attenuated using the 1 × 2 × 1 or 1 × 1 × 2 arrangements of resonant inclusions, while the use of engineered inclusions, especially, further enhances the wave suppression while using approximately 40% less mass than control inclusions.

Additionally, it is evident that the results measured among the engineered inclusions with different constraints (i.e. A, B, and C) are not significantly different for the improved inclusion arrangements characterized in Fig. 4(b) with 6 cm spacing in the x-axis, or Fig. 8(b) for 1 × 1 × 2 arrangement. This is despite the fact that the constraints realized for the inclusions are specifically varied around the theoretically ideal point of criticality, as discussed and characterized in Section 2. Consequently, an additional finding derived from these experimental results is that the utilization of multiple engineered and constrained inclusions in resonant metamaterials leads to a robust enhancement of the broadband vibroacoustic energy. The robustness means that constraints are not strongly sensitive to non-ideal parameters away from criticality, at least in considering the macroscopic properties of the resonant metamaterials. Thus, while utilizing the precise critical point constraint phenomena for shock attenuation is preferred [19], this research finds that generating enhanced vibroacoustic energy attenuation properties in resonant metamaterials is less reliant upon precision of inclusion fabrication and assembly, thus leading to robust enhancement of the energy suppression.

4. Conclusions

In this report, multiple, engineered, and constrained inclusions embedded in poroelastic foam, to realize resonant metamaterials, are experimentally characterized for the ability to enhance wave energy

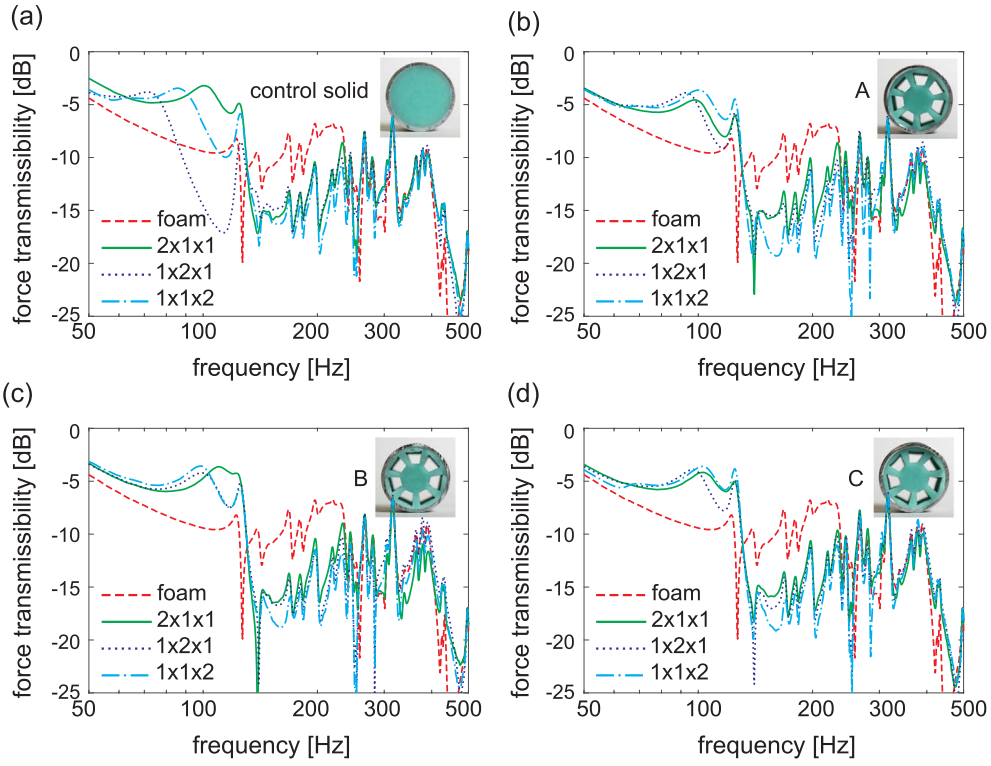

Fig. 7. Force transmissibility for (a) control inclusions (b) engineered Type A inclusions (c) Type B inclusions and (d) Type C inclusions.

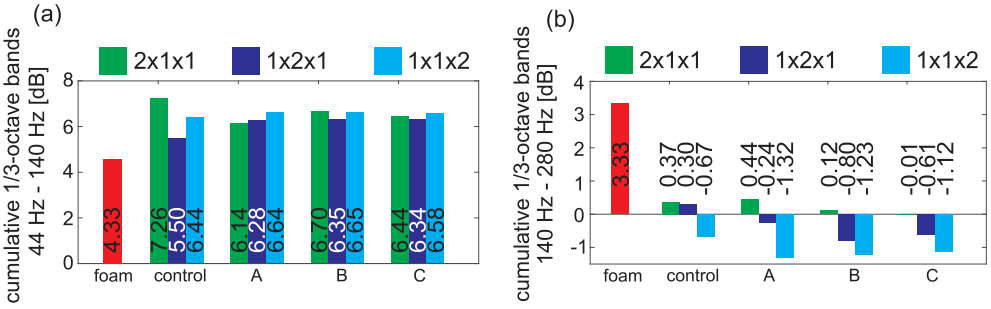

Fig. 8. Cumulative 1/3-octave bands for (a) lower band of 44–140 Hz and (b) upper band of 140–280 Hz.

attenuation properties when compared to the foam itself and when compared to metamaterials with lumped mass inclusions. It is discovered that critically constrained metamaterials more greatly suppress broadband elastic waves when inclusions are spaced apart in the axis of wave propagation. Arrangements of two inclusions are also shown to be more effective to enhance the attenuation properties when the inclusions are arranged perpendicular to the direction of wave propagation. Critically constrained inclusions within the metamaterials are seen to be as or more effective at attenuating vibroacoustic energy than conventional solid inclusions. Moreover, the engineered inclusions utilize approximately 40% less mass than the solid inclusions while providing robust, broadband vibroacoustic energy attenuation properties when the applied inclusion constraint deviates from ideal design parameters. This robustness means that leveraging critical constraints is not a parameter sensitive phenomenon, and can still be effective even when it is not ideally tuned.

Acknowledgements

R.L.H. acknowledges start-up funds from the Department of Mechanical and Aerospace Engineering at The Ohio State University (OSU). J.B. acknowledges support from the OSU College of Engineering Honors Research Scholarship.

References

[1] Crocker MJ. Introduction to interior transportation noise and vibration sources. In: Crocker MJ, editor. Handbook of noise and vibration control. Hoboken, New Jersey: John Wiley and Sons Inc.; 2007.
[2] Bies DA, Hansen CH. Engineering noise control: theory and practice. London: Spon Press; 2006.
[3] Allard JF, Atalla N. Propagation of sound in porous media: modelling sound absorbing materials. Chichester: John Wiley and Sons; 2009.
[4] Cremer L, Heckl M, Petersson BAT. Structure-borne sound: structural vibrations and sound radiation at audio frequencies. Berlin: Springer; 2005.
[5] Baravelli E, Ruzzene M. Internally resonating lattices for bandgap generation and low-frequency vibration control. J Sound Vib 2013;332:6562–79.
[6] Zhu R, Liu XN, Hu GK, Sun CT, Huang GL. A chiral elastic metamaterial beam for broadband vibration suppression. J Sound Vib 2014;333:2759–73.
[7] Acar G, Yilmaz C. Experimental and numerical evidence for the existence of wide and deep phononic gaps induced by inertial amplification in two-dimensional solid structures. J Sound Vib 2013;332:6389–404.
[8] Nouh M, Aldraihem O, Baz A. Wave propagation in metamaterial plates with periodic local resonances. J Sound Vib 2015;341:53–73.
[9] Liu Z, Zhang X, Mao Y, Zhu YY, Yang Z, Chan CT, et al. Locally resonant sonic materials. Science 2000;289:1734–6.
[10] Shan S, Kang SH, Wang P, Qu C, Shian S, Chen ER, et al. Harnessing multiple folding mechanisms in soft periodic structures for tunable control of elastic waves. Adv Funct Mater 2014;24:4935–42.
[11] Pal RK, Rimoli J, Ruzzene M. Effect of large deformation pre-loads on the wave properties of hexagonal lattices. Smart Mater Struct 2016;25:054010.
[12] Shan S, Kang SH, Raney JR, Wang P, Fang L, Candido F, et al. Multistable architected materials for trapping elastic strain energy. Adv Mater 2015;27:4296–301.

[13] Schaeffer M, Ruzzene M. Dynamic reconfiguration of magnto-elastic lattices. CR Mec 2015;343:670–9.
[14] Florijn B, Coulais C, van Hecke M. Programmable mechanical metamaterials. Phys Rev Lett 2014;113:175503.
[15] Antoniadis I, Chronopoulos D, Spitas V, Koulocheris D. Hyper-damping peroperties of a stiff and stable linear oscillator with a negative stiffness element. J Sound Vib 2015;346:37–52.
[16] Bažant ZP, Cedolin L. Stability of structures: elastic, inelastic, fracture, and damage theories. Hackensack, New Jersey: World Scientific Publishing Co.; 2010.
[17] Wang YC, Ludwigson M, Lakes RS. Deformation of extreme viscoelastic metals and composites. Mater Sci Eng, A 2004;370:41–9.
[18] Wojnar CS, le Graverend JB, Kochmann DM. Broadband control of the viscoelasticity of ferroelectrics via domain switching. Appl Phys Lett 2014;105:162912.
[19] Bishop J, Dai Q, Song Y, Harne RL. Resilience to impact by extreme energy absorption in lightweight material inclusions constrained near a critical point. Adv Eng Mater 2016;18:1871–6.
[20] Fuller CR, Harne RL. Passive distributed vibration absorbers for low frequency noise control. Noise Control Eng. J. 2010;58:627–35.
[21] Idrisi K, Johnson ME, Theurich D, Carneal JP. A study on the characteristic behavior of mass inclusions added to a poro-elastic layer. J Sound Vib 2010;329:4136–48.
[22] Idrisi K, Johnson ME, Toso A, Carneal JP. Increase in transmission loss of a double panel system by addition of mass inclusions to a poro-elastic layer: a comparison between theory and experiment. J Sound Vib 2009;323:51–66.
[23] Doutres O, Atalla N. Transfer matrix modeling and experimental validation of cellular porous material with resonant inclusions. J Acoust Soc Am 2015;137:3502–13.
[24] Groby JP, Lagarrigue C, Brouard B, Dazel O, Tournat V. Using simple shape three-dimensional rigid inclusions to enhance porous layer absorption. J Acoust Soc Am 2014;136:1139–48.
[25] Harne RL, Song Y, Dai Q. Trapping and attenuating broadband vibroacoustic energy with hyperdamping metamaterials. Extreme Mech Lett 2017;12:41–7.
[26] Weisser T, Groby JP, Dazel O, Gaultier F, Deckers E, Futatsugi S, et al. Acoustic behavior of a rigidly backed poroelastic layer with periodic resonant inclusions by a multiple scattering approach. J Acoust Soc Am 2016;139:617–29.
[27] Weisser T, Groby JP, Dazel O, Schwan L. High broadband absorption of acoustic waves by elastic-framed metaporous layer. In: Proceedings of the 10th international congress on advanced electromagnetic materials in microwaves and optics - metamaterials 2016, Crete, Greece; 2016. p. 322–4.
[28] Wang P, Casadei F, Shan S, Weaver JC, Bertoldi K. Harnessing buckling to design tunable locally resonant acoustic metamaterials. Phys Rev Lett 2014;113:014301.
[29] Virgin LN. Vibration of axially loaded structures. Cambridge: Cambridge University Press; 2007.
[30] Panneton R, Olny X. Acoustical determination of the parameters governing viscous dissipation in porous media. J Acoust Soc Am 2006;119:2027–40.
[31] ASTM International. Standard test method for impedance and absorption of acoustical materials using a tube, two microphones and a digital frequency analysis system. ASTM E1050-12; 2012.
[32] ASTM International. Standard test method for measurement of normal incidence sound transmission of acoustical materials based on the transfer matrix method. E2611-09; 2009.
[33] Atalla N, Panneton R. Acoustic absorption of macro-perforated porous materials. J Sound Vib 2001;243:659–78.
[34] Lagarrigue C, Groby JP, Tournat V, Dazel O, Umnova O. Absorption of sound by porous layers with embedded periodic arrays of resonant inclusions. J Acoust Soc Am 2013;134:4670–80.